Revision of Convection and Vertical Diffusion Schemes in the NCEP Global Forecast System

JONGIL HAN

Wyle Information Systems LLC, and National Centers for Environmental Prediction/Environmental Modeling Center, Camp Springs, Maryland

HUA-LU PAN

National Centers for Environmental Prediction/Environmental Modeling Center, Camp Springs, Maryland

(Manuscript received 12 October 2010, in final form 14 February 2011)

ABSTRACT

A new physics package containing revised convection and planetary boundary layer (PBL) schemes in the National Centers for Environmental Prediction's Global Forecast System is described. The shallow convection (SC) scheme in the revision employs a mass flux parameterization replacing the old turbulent diffusion-based approach. For deep convection, the scheme is revised to make cumulus convection stronger and deeper to deplete more instability in the atmospheric column and result in the suppression of the excessive grid-scale precipitation. The PBL model was revised to enhance turbulence diffusion in stratocumulus regions. A remarkable difference between the new and old SC schemes is seen in the heating or cooling behavior in lower-atmospheric layers above the PBL. While the old SC scheme using the diffusion approach produces a pair of layers in the lower atmosphere with cooling above and heating below, the new SC scheme using the mass-flux approach produces heating throughout the convection layers. In particular, the new SC scheme does not destroy stratocumulus clouds off the west coasts of South America and Africa as the old scheme does. On the other hand, the revised deep convection scheme, having a larger cloud-base mass flux and higher cloud tops, appears to effectively eliminate the remaining instability in the atmospheric column that is responsible for the excessive grid-scale precipitation in the old scheme. The revised PBL scheme, having an enhanced turbulence mixing in stratocumulus regions, helps prevent too much low cloud from forming. An overall improvement was found in the forecasts of the global 500-hPa height, vector wind, and continental U.S. precipitation with the revised model. Consistent with the improvement in vector wind forecast errors, hurricane track forecasts are also improved with the revised model for both Atlantic and eastern Pacific hurricanes in 2008.

1. Introduction

To improve forecast performance, the model physics in the National Centers for Environmental Prediction's (NCEP) Global Forecast System (GFS) model, the operational medium-range forecast model at NCEP, is under continual development. However, few significant changes to the convection and vertical diffusion schemes have been made since 2001, due to the difficulty of satisfying the concomitant requirement for a careful consideration of interactions among the model physics packages. In this paper, we present and evaluate revised shallow and deep convection and vertical diffusion schemes based on advanced physical parameterizations.

One of the long-standing problems in the GFS was a systematic underestimation of stratocumulus clouds, especially over nearshore regions in the eastern Pacific and Atlantic Oceans (Fig. 1). This problem has been attributed to the shallow convection (SC) scheme, which uses a turbulent diffusion approach. On the other hand, the GFS has also suffered from so-called gridpoint storms (excessively heavy precipitation at the grid scale) during the convective season, which was another long-standing problem in the GFS forecasts. Although this revision has initially been made in pursuit of fixing these long-standing problems, it has also proved to increase

Corresponding author address: Jongil Han, WWB, Rm. 207, 5200 Auth Rd., Camp Springs, MD 20746.
E-mail: jongil.han@noaa.gov

DOI: 10.1175/WAF-D-10-05038.1

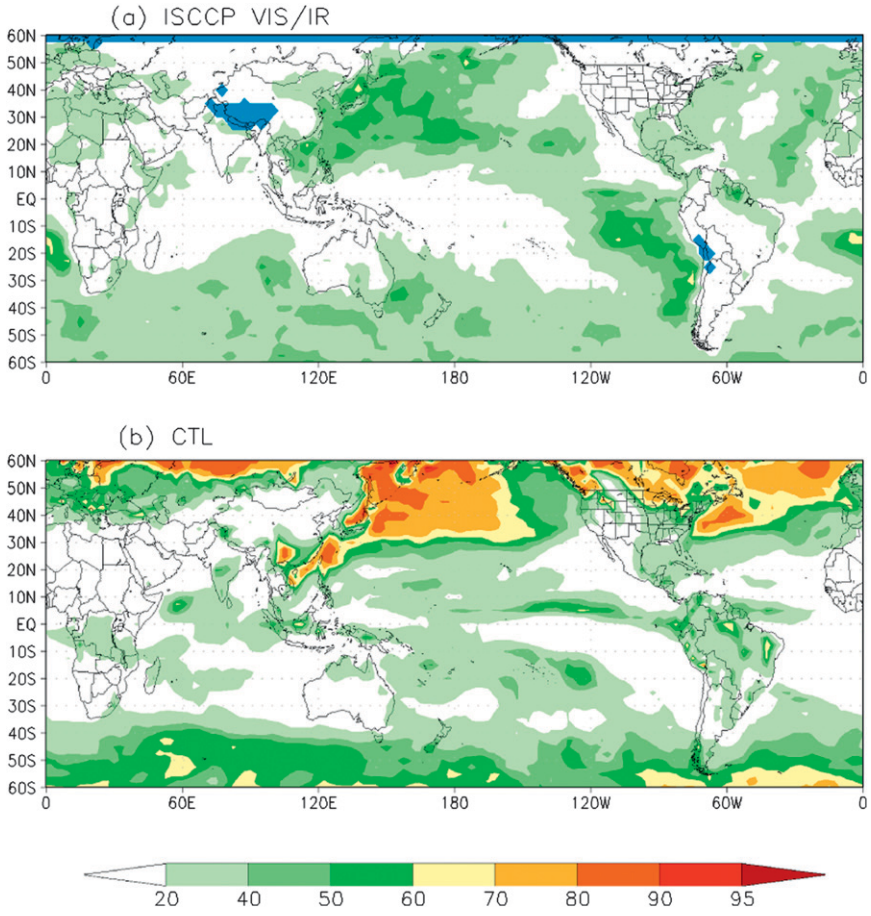

FIG. 1. Monthly mean low cloud cover (%) for January 2003 from (a) the International Satellite Cloud Climatology Project (ISCCP; Rossow and Schiffer 1991) VIS/IR satellite observations (regions with no data available are shown in blue) and (b) a control simulation using the old shallow convection scheme.

the model forecast skill as shown later in this paper. This led us to implement the revised schemes operationally into the GFS as of late July 2010.

The biggest change made was in the shallow convection scheme. The old operational SC scheme in the GFS used a simple turbulent eddy diffusion approach with a specified eddy diffusivity profile for the transport of sensible heat and moisture within convectively unstable layers, following the procedure proposed by Tiedtke et al. (1988). While this scheme has been successful in removing unrealistic moisture accumulation in the layer below the inversion by means of the additional diffusion of heat and moisture, it tends to deplete real stratocumulus clouds as seen in Fig. 1. To better represent the physical processes of shallow convection, in this study we have developed a bulk mass-flux parameterization. While the new SC scheme is based on the simplified Arakawa–Schubert (SAS) convection scheme (Pan and Wu 1995) used operationally in the GFS model for deep cumulus convection, many aspects in the SAS scheme such as cloud-base mass flux, entrainment, and detrainment specifications, have been modified to accommodate the SC. On the other hand the SAS deep convection scheme has been revised in order to suppress the unrealistic gridpoint storms, which are believed to result from the convective parameterization not fully eliminating the instability and consequently causing explicit convective ascent to occur on the grid scale. To this end, the scheme was modified to make the cumulus convection stronger and deeper.

The old operational nonlocal planetary boundary layer (PBL) scheme in the NCEP GFS [the so-called Medium-Range Forecast (MRF) PBL model] proposed by Troen and Mahrt (1986) and implemented by Hong and Pan (1996) has been widely used for vertical diffusion because it not only provided a realistic development of a well-mixed layer despite its simplicity, but has also produced consistent improvement in the skill levels of

precipitation forecasts over the continental United States (Caplan et al. 1997). However, this scheme is optimized for the simulation of dry boundary layers and tends to produce too much low cloudiness. To increase vertical diffusion in the cloudy region of the lower troposphere, therefore, a stratocumulus cloud-top-driven vertical diffusion scheme (Lock et al. 2000) has been incorporated into the MRF PBL model along with the new SC scheme.

Details of these revisions are described below in section 2. In section 3, we evaluate the impacts of the model physics changes. Finally, in section 4 we summarize our results and draw some conclusions.

2. Description of model physics changes

a. Convection

1) Shallow convection

A turbulent eddy diffusion approach proposed by Tiedtke et al. (1988) was used for the SC in the previous GFS. The scheme first looks for a convectively unstable layer, defined as the layer between the lifting condensation level (LCL) and the first neutral level above the LCL (but no higher than about the 700-hPa level), as a parcel originating in the second model layer is lifted. Then, vertical mixing of the heat and moisture within the convectively unstable layer is simulated using a parabolic eddy diffusivity profile with a maximum value of 5 $m^2\ s^{-1}$. But this diffusion approach for the SC has been proved to be physically unreasonable. For example, a mass-flux analogy for the vertical local turbulent diffusion [i.e., zero vertical velocity skewness; de Roode et al. (2000)] indicates that the vertical turbulent transport can be represented by an updraft and downdraft, with each occupying half the area in a given model grid box. For cumulus convection on the other hand, the mass-flux approach assumes a near-zero fractional area for the updraft in a given grid box, a more realistic assumption for the SC. With the mass-flux approach, therefore, the cloud environment is dominated by subsidence resulting in environmental warming and drying, while the environmental change in the case of the eddy diffusion approach depends on the vertical profile shapes of the environmental variables.

Since the SC mass-flux parameterization developed in this study is based on the SAS deep convection scheme that can be found in Pan and Wu (1995), we present here only the relevant equations that distinguish between the shallow and deep convection schemes. As in the SAS scheme, a simple cloud model for the SC is used to describe the mass, moist static energy, and moisture within the updraft:

$$\frac{1}{\eta}\frac{\partial \eta}{\partial z} = \varepsilon - \delta, \tag{1}$$

$$\frac{\partial(\eta s)}{\partial z} = (\varepsilon \bar{s} - \delta s)\eta, \quad \text{and} \tag{2}$$

$$\frac{\partial[\eta(q_v + q_l)]}{\partial z} = \eta[\varepsilon \bar{q}_v - \delta(q_v + q_l) - r], \tag{3}$$

where η represents the mass flux normalized by the mass flux at the cloud base; ε the entrainment rate; δ the detrainment rate; s the moist static energy; q_v and q_l the vapor and liquid water mixing ratio in the updraft, respectively; r the precipitation; and the overbar the horizontal average. For the SC it is assumed that no convective-scale downdrafts exist.

The vertical integration of Eqs. (1)–(3) requires a knowledge of the cloud-base mass flux and mass entrainment and detrainment. The cloud-base mass flux m_b is given as a function of the surface buoyancy flux (Grant 2001); that is,

$$m_b = 0.03\rho w_*, \tag{4}$$

where ρ is the air density and w_* is the convective velocity scale defined by

$$w_* = [(g/T_0)(\overline{w'\theta'_v})_0 h]^{1/3}, \tag{5}$$

where h is the PBL height, g gravity, T_0 the reference temperature, and $(\overline{w'\theta'_v})_0$ the surface virtual kinematic heat flux. This differs from the SAS deep convection scheme, which uses the quasi-equilibrium closure method of Arakawa and Schubert (1974) where the destabilization of an air column by the large-scale atmospheric processes is nearly balanced by the stabilization due to the cumulus.

While the convection starting level (CSL) in deep convection is defined as the level of maximum moist static energy between the surface and 700-hPa level, in the SC it is assumed to be the level of maximum moist static energy within the PBL. The level of free convection (LFC) is used as the cloud base when a parcel is taken upward. The cloud top is initially assumed to be the first neutral level encountered as the parcel is further lifted from the cloud base. A cloud thickness criterion distinguishes shallow from deep convection. Deep convection is checked first: if the cloud is thicker than 150 hPa, deep convection is activated; otherwise, the convection is treated as being shallow. The cloud top in the SC is limited to $P/P_s = 0.7$ (where P is the layer pressure and the subscript s represents the ground surface). As

described later in section 2a(3), the cloud top is increased for both deep and shallow convection by convective overshooting.

Large eddy simulation (LES) studies by Siebesma and Cuijpers (1995) indicate that the fractional entrainment and detrainment rates for the SC are one order of magnitude larger than the values used in most existing deep convection schemes. The LES study by Siebesma et al. (2003) indicates that a typical value for the fractional entrainment rate is $\varepsilon \sim 2.0 \times 10^{-3}$ m^{-1} near the cloud base, which agrees with other LES studies (Siebesma and Cuijpers 1995; Grant and Brown 1999) and observations (Raga et al. 1990), and that the entrainment rate behaves as

$$\varepsilon = c_e \frac{1}{z}, \tag{6}$$

where z is the height and the empirical coefficient $c_e = 1.0$. In this study, Eq. (6) with a smaller value of $c_e = 0.3$ is used for the SC entrainment rate. We find that the larger value $c_e = 1.0$ tends to reduce the shallow cumulus-top height too much and to consequently increase cloud water too much in the lower atmosphere due to a reduced extent for shallow convection. We reached an optimum value of $c_e = 0.3$ based on the vertical distribution of cloud water. The detrainment rate is assumed to be a constant and is given as the entrainment rate at the cloud base. In this way, the mass flux decreases with height above the cloud base while it increases with height below the cloud base, which is consistent with the aforementioned LES studies. The liquid water in the updraft layer is allowed to be detrained from every layer into the convective rain and grid-scale cloud water with conversion parameters of 0.002 m^{-1} and 5.0×10^{-4} m^{-1}, respectively.

The feedback of cumulus convection into the large-scale environment is accomplished via the compensating subsidence in the environment and the entrainment and detrainment processes between the cloud and the environment. Although we allow precipitation processes in the SC, initial tests indicate that the precipitation from the SC is quite small.

2) DEEP CONVECTION

Many changes have also been made in the SAS deep convection scheme. As mentioned in the introduction, the old deep convection scheme does not appear to fully eliminate the instability and consequently an explicit convective ascent occurs at the grid scale, producing unrealistically heavy precipitation. Random cloud-top selection in the old SAS scheme (Moorthi et al. 2001) is no longer used, since it tends to make the cloud top lower on average and appears to weaken convection strength. To further increase convection strength, the maximum allowable cloud-base mass flux [M_{bmax}, 0.1 kg (m^2 s^{-1})$^{-1}$ in the old SAS scheme] is increased by defining a local Courant–Friedrichs–Lewy (CFL) criterion to be satisfied (Jakob and Siebesma 2003); that is,

$$M_{\mathrm{bmax}} = \frac{\Delta p}{g \Delta t}, \tag{7}$$

where Δp and Δt are depth of the model layer at the cloud base and the model time step, respectively, and g is the gravity. An initial test indicates that the M_{bmax} from Eq. (7) can be about 5 times larger than that in the old SAS scheme with T382 horizontal resolution (triangular truncation at wavenumber 382; about 35 km at the equator).

Unlike the old SAS scheme, the revised SAS scheme specifies finite entrainment and detrainment rates for heat, moisture, and momentum above the cloud base. Following Bechtold et al. (2008), the entrainment is specified as

$$\varepsilon = \varepsilon_0 F_0 + d_1(1 - \mathrm{RH}) F_1 \quad \text{and}$$

$$F_0 = \left(\frac{\overline{q}_s}{\overline{q}_{\mathrm{sb}}}\right)^2, \quad F_1 = \left(\frac{\overline{q}_s}{\overline{q}_{\mathrm{sb}}}\right)^3, \tag{8}$$

where ε_0 is the entrainment rate at the cloud base; RH the environmental relative humidity; d_1 a tunable parameter of $O(10^{-4})$; q_s and q_{sb} the saturation specific humidities at the parcel level and the cloud base, respectively; and F_0 and F_1 are dimensionless vertical scaling functions that decrease strongly with height. Equation (8) indicates that a drier environment (lower RH) increases the entrainment, suppressing convection.

Similar to the SC scheme, the entrainment rate in subcloud layers is given to be inversely proportional to height but with a smaller coefficient of $c_e = 0.1$ in Eq. (6). The detrainment rate is assumed to be a constant at all layers and equal to the entrainment rate value at the cloud base, which is $O(10^{-4})$. The liquid water in the updraft layer is assumed to be detrained from the layers above the level of the minimum moist static energy into the grid-scale cloud water with a conversion parameter of 0.002 m^{-1}, which is the same as the rain conversion parameter.

3) MOMENTUM TRANSPORT, TRIGGER FUNCTION, AND CONVECTIVE OVERSHOOTING

The effects of the convection-induced pressure gradient force on cumulus momentum transport (Zhang and Wu 2003; Han and Pan 2006) are included in both

the deep and shallow convection parameterizations. Note that momentum transport is absent in the old operational SC scheme. A cloud model to describe, respectively, the momentum within the updraft and momentum feedback to the environment can be expressed as

$$\frac{\partial \mathbf{V}}{\partial z} = \varepsilon(\overline{\mathbf{V}} - \mathbf{V}) + f_1 \frac{\partial \overline{\mathbf{V}}}{\partial z} \quad \text{and} \tag{9}$$

$$\frac{\partial \overline{\mathbf{V}}}{\partial t} = (1 - f_1) M \frac{1}{\rho} \frac{\partial \overline{\mathbf{V}}}{\partial z} + \delta(\mathbf{V} - \overline{\mathbf{V}}), \tag{10}$$

where $\mathbf{V}$ is the horizontal wind vector, M the updraft mass flux, and f_1 an empirical constant representing the effects of the convection-induced pressure gradient force that weakens the cumulus momentum exchange. In the old operational SAS scheme, f_1 is 0, implying a full momentum exchange in the cumulus convection. Based on Zhang and Wu's (2003) cloud-resolving model results, in this study f_1 is set to be 0.55 for both the deep and shallow convection schemes, implying that the cumulus momentum exchange is reduced by about 55% compared to a full exchange.

The triggering condition in the old SAS scheme was that a parcel lifted from the CSL without entrainment must reach its LFC within 150 hPa of ascent, which crudely represents an upper limit of convective inhibition. The fixed value of 150 hPa is now slightly modified to vary within the range 120–180 hPa, in proportion to the large-scale vertical velocity. This modification is intended to produce more convection in large-scale convergent regions but less convection in large-scale subsidence regions. Another important triggering mechanism is to include the effects of environmental humidity in the subcloud layer. Since the scheme allows entrainment in the subcloud layers, the LFC becomes higher if drier environmental air entrains into the parcel. In the old operational trigger, the vertical model layer difference between the LFCs with and without subcloud layer entrainment must be less than two, taking into account convection inhibition due to the existence of dry layers below the cloud base. This may become a serious deficiency as the vertical model resolution changes. In other words, higher (lower) vertical model resolution might give rise to less (more) convection triggering. In the revision, therefore, we use pressure difference instead of model layer difference for the LFC difference. The threshold value for the pressure difference that triggers convection is set to be 25 hPa in both the deep and shallow convection schemes.

The cloud parcel might overshoot beyond the level of neutral buoyancy due to its inertia, eventually stopping at the cloud top (Stull 1988). The cloud work function [CWF, defined as work done by the buoyancy force in a cloud; Arakawa and Schubert (1974)] can be used to model the overshoot. In this study, the overshooting is stopped at the height where a parcel lifted from the neutral buoyancy level with energy equal to 10% of the CWF will first reach zero energy. This convective overshoot is applied to both the deep and shallow convection schemes.

b. Vertical diffusion

Readers are urged to refer to Troen and Mahrt (1986, hereafter TM) and Hong and Pan (1996) for a detailed description of the MRF PBL model. Here, we present only that part relevant to the MRF PBL scheme. As mentioned in the introduction, in the revision a cloud-top-driven vertical diffusion scheme is incorporated into the MRF PBL model to increase vertical diffusion in the cloudy regions of the lower troposphere, simplified after Lock et al. (2000). In the revised model, the vertical heat flux is given by

$$\overline{w'\theta'} = -(K_h^{\text{surf}} + K_h^{\text{Sc}}) \frac{\partial \overline{\theta}}{\partial z} + K_h^{\text{surf}} \gamma_h \tag{11a}$$

in the daytime well-mixed boundary layers, and

$$\overline{w'\theta'} = -[K_h(\text{Ri}) + K_h^{\text{Sc}}] \frac{\partial \overline{\theta}}{\partial z} \tag{11b}$$

in the atmospheric layers above the mixed layer and nighttime stable boundary layers, where K_h^{surf} and K_h^{Sc} are the surface and cloud-top-driven eddy diffusivities, respectively; γ_h is the nonlocal countergradient mixing term due to large nonlocal convective eddies; and $K_h(\text{Ri})$ is the mixing coefficient based on the local Richardson number (described later). The MRF PBL model does not have K_h^{Sc} in Eq. (11) and, thus, the revised model displays a larger vertical heat flux in the stratocumulus region compared to the MRF PBL scheme.

For surface-driven diffusion, the vertical diffusivity for momentum as proposed by TM is given by

$$K_m^{\text{surf}} = \kappa w_s z \left(1 - \frac{z}{h}\right)^2, \tag{12}$$

where $\kappa = 0.4$ is the von Kármán constant, z is the distance from the surface, and h is the PBL height. The velocity scale w_s is represented by the value scaled at the top of the surface layer; that is,

$$w_s = (u_*^3 + 7\alpha\kappa w_*^3)^{1/3}, \tag{13}$$

where u_* is the surface friction velocity, α is the ratio of the surface layer height to the PBL height (specified as 0.1), and w_* is the convective velocity scale defined in Eq. (5). The eddy diffusivity for heat is derived from K_m^{surf} using the Prandtl number (Pr); that is, $K_h^{\text{surf}} = \text{Pr}^{-1} K_m^{\text{surf}}$. With the nonlocal countergradient mixing for heat, TM obtains the Prandtl number at the top of the surface layer ($z = \alpha h$) as

$$\text{Pr} = \frac{\Phi_h}{\Phi_m} + b\alpha\kappa, \tag{14}$$

where Φ_h and Φ_m are the nondimensional gradient functions for heat and momentum, respectively, and b (=6.5) is a proportionality coefficient. The Prandtl number is assumed to be constant over the whole PBL.

Following Lock et al. (2000), the stratocumulus-top-driven diffusivity is given by

$$K_h^{\text{Sc}} = 0.85\kappa V_{\text{Sc}} \frac{(z - z_b)^2}{h_b - z_b}\left(1 - \frac{z - z_b}{h_b - z_b}\right)^{1/2}, \tag{15}$$

where h_b is the level of the stratocumulus top and z_b is the level below the cloud base to which the top-driven mixing extends. The parameter V_{Sc} represents a cloud-top entrainment velocity scale, defined by

$$V_{\text{Sc}}^3 = V_{\text{rad}}^3 + V_{\text{br}}^3, \tag{16}$$

where V_{rad} and V_{br} are the radiative cooling and buoyancy reversal terms, respectively. The buoyancy reversal term is neglected in this study. The radiative cooling term is given by

$$V_{\text{rad}}^3 = \frac{g}{\theta_0}(h_b - z_b)\Delta R/(\rho c_p), \tag{17}$$

where ΔR is the radiative flux jump at the cloud top, ρ is air density, and c_p the specific heat at constant pressure. To have an accurate measure of the buoyancy of parcels descending adiabatically from cloud top or ascending adiabatically from the surface, in the revision we use the virtual liquid water potential temperature θ_{vl}[$=\theta_l(1 + 0.608q_t)$, where $\theta_l = \theta - (L/c_p)q_l$, $q_t = q_v + q_l$, q_v and q_l are the vapor and liquid water mixing ratios, and where L is the latent heat of vaporization of water] rather than the virtual potential temperature θ_v. A parcel descent from the cloud top to determine z_b is made by perturbing the cloud-top θ_{vl} by an amount equal to the cloud-top radiative cooling rate, multiplied by an assumed cloud-top residence time scale of 500 s (Lock et al. 2000). The grid level at which this parcel's θ_{vl} exceeds that of the environment is used to estimate z_b. The presence of stratocumulus is diagnosed by moving a parcel downward from the top of any cloud layer having a liquid water content greater than a threshold value of $q_l = 3.5 \times 10^{-5}$ kg kg^{-1}. This diagnosis is restricted to the lowest 2.5 km of the model domain. Then, the cloud-top h_b is defined as the level with the highest radiative cooling rate in the cloud layer.

The cloud-top entrainment flux is given by

$$-\overline{(w'\theta_v')}_{h_b} = c\frac{\Delta R}{\rho c_p}, \tag{18}$$

where c is a constant. In this study we use $c = 0.2$ following Moeng et al. (1999), implying that 20% of the total radiative flux jump occurs across the cloud top. When the conditions for cloud-top entrainment instability (CTEI) are met, however, the stratocumulus-top-driven diffusion is enhanced by increasing c to 1.0. The conditions for CTEI are given by (Randall 1980; Deardorff 1980)

$$c_p\Delta\theta_e/L\Delta q_t > c_1, \tag{19}$$

where $\Delta\theta_e$ and Δq_t are the jumps in equivalent potential temperature and total water content across the cloud top and a constant $c_1 = 0.7$ (MacVean and Mason 1990) is used.

For the atmospheric layers above the daytime mixed layer and nighttime stable boundary layer, we use a local closure scheme (Louis et al. 1982), where the diffusivity coefficients for momentum and heat are expressed in terms of the mixing length l; stability functions $f_{m,h}(\text{Ri})$; and magnitude of the vertical wind shear $|\partial U/\partial z|$; that is,

$$K_{m,h}(\text{Ri}) = l^2 f_{m,h}(\text{Ri})\left|\frac{\partial U}{\partial z}\right|. \tag{20}$$

In Eq. (20) the mixing length l is given by

$$\frac{1}{l} = \frac{1}{kz} + \frac{1}{l_0}, \tag{21}$$

where the asymptotic length scale l_0 is assumed to be 30 m for stable conditions and 150 m for unstable conditions. The stability functions $f_{m,h}(\text{Ri})$ are represented as a function of the local gradient Richardson number Ri. For stable conditions ($\text{Ri} \geq 0$),

$$f_h(\text{Ri}) = 1/(1 + 5\text{Ri})^2, \tag{22}$$

with

$$\mathrm{Pr} = 1 + 2.1\mathrm{Ri}. \quad (23)$$

For unstable conditions ($\mathrm{Ri} < 0$),

$$f_h(\mathrm{Ri}) = 1 + \frac{8|\mathrm{Ri}|}{1 + 1.286|\mathrm{Ri}|^{1/2}} \quad \text{and} \quad (24)$$

$$f_m(\mathrm{Ri}) = 1 + \frac{8|\mathrm{Ri}|}{1 + 1.746|\mathrm{Ri}|^{1/2}}. \quad (25)$$

The background diffusivity in the GFS for heat and moisture exponentially decreases with height from 1.0 $m^2\ s^{-1}$. To avoid excessive erosion of stratocumulus along coastal areas, the background diffusivity in the lower inversion layers is further reduced to 30% of that at the surface (i.e., 0.3 $m^2\ s^{-1}$) in the revision. On the other hand, the background diffusivity for momentum has been substantially increased everywhere to 3.0 $m^2\ s^{-1}$, which helps reduce the wind forecast errors.

c. Cloud fraction

We also modified the old GFS cloud cover calculation because it tends to produce too much low cloud over the entire globe with the new SC scheme. Following Xu and Randall (1996), the fractional cloud cover within a grid box (σ) is given by

$$\sigma = \mathrm{RH}^{k_1}\left(1 - \exp\left\{-\frac{k_2 q_l}{[(1-\mathrm{RH})q_s]^{k_3}}\right\}\right), \quad (26)$$

where k_1, k_2, and k_3 are empirical coefficients. Using data produced from explicit simulations of the observed tropical cloud systems, Xu and Randall have obtained empirical values of k_1, k_2, and k_3 that are 0.25, 100, and 0.49, respectively. In the previous GFS, values of $k_1 = 0.25$, $k_2 = 2000$, and $k_3 = 0.25$ are used to increase cloud cover because the old SC scheme is too efficient in destroying stratocumulus clouds. Now that the new SC scheme in this study can produce sufficient low clouds, the original empirical values of Xu and Randall (i.e., $k_1 = 0.25$, $k_2 = 100$, and $k_3 = 0.49$) are used.

3. Test and evaluation

a. Coupled model test

To see the broad features of the impacts of these changes in the convection and PBL schemes we first employ the NCEP atmosphere–ocean Coupled Forecasting System (CFS; Wang et al. 2005; Saha et al. 2006), where the GFS is used as the atmospheric model and the oceanic component is the Geophysical Fluid Dynamics Laboratory Modular Ocean Model version 3 (Pacanowski and Griffies 1998). The GFS used in this test has 64 vertical sigma-pressure hybrid layers and T126 horizontal resolution (about 100 km at the equator). The CFS run was initialized at 0000 UTC 16 December 2002 and ran for 45 days. The CFS forecasts during the preceding 15 days (a spinup period) have been discarded from the analysis, and forecast results during the remaining 1-month period are presented. An evaluation using a longer CFS run would be desirable, but will be left for a future study.

Figure 2a shows that much more realistic low cloud distributions are obtained in comparison to the control run as the new SC scheme is introduced along with the revised PBL scheme. In particular, the improvement in stratocumulus formation in the regions off the west coasts of the Americas and Africa is remarkable. Without an enhanced diffusion by stratocumulus-cloud-top-driven turbulence in the PBL scheme, too much low cloud cover is formed as seen in Fig. 2b. In Fig. 3, we display the distribution of cloud water averaged over 10°S–10°N to see the effects of the SC scheme. With the SC parameterization turned off (Fig. 3b), cloud water is accumulated in the lower-atmospheric layers just above the PBL, giving rise to an unrealistically large low cloud coverage. As shown in Fig. 3a, on the other hand, the old SC scheme using a turbulent diffusion approach strongly depletes the lower-layer cloud water and diffuses it up to the upper layers, forming a significant amount of cloud water near the 750–600-hPa layers. This is why stratocumulus clouds are lacking with the old SC scheme. The new SC scheme (Fig. 3c) shows an intermediate cloud water distribution between that with no SC scheme and that from the old SC scheme.

Figure 4 displays zonally averaged heating rates due to the SC. The old SC scheme (Fig. 4a) produces cooling at 700–850 hPa and heating below that level, showing the strongest cooling and heating over the tropical regions. This is a typical feature seen when a parabolic diffusivity profile is applied to stable layers. The upper limit of the cooling layers (i.e., about 700 hPa) is associated with the fact that the shallow cloud top in the old SC scheme is limited to sigma level 0.7. For the new SC scheme (Fig. 4b), however, the entire lower atmosphere is heated, especially over tropical and subtropical areas (where most of the shallow cumulus convection occurs) by the dominant environmental subsidence warming typical of convection schemes using the mass-flux approach. The slight cooling near the surface with the new SC scheme could be caused by the detrainment of rising air parcels cooled adiabatically while subsidence heating would be very small near the surface due to a small mass flux. Figure 5 displays a global distribution for the

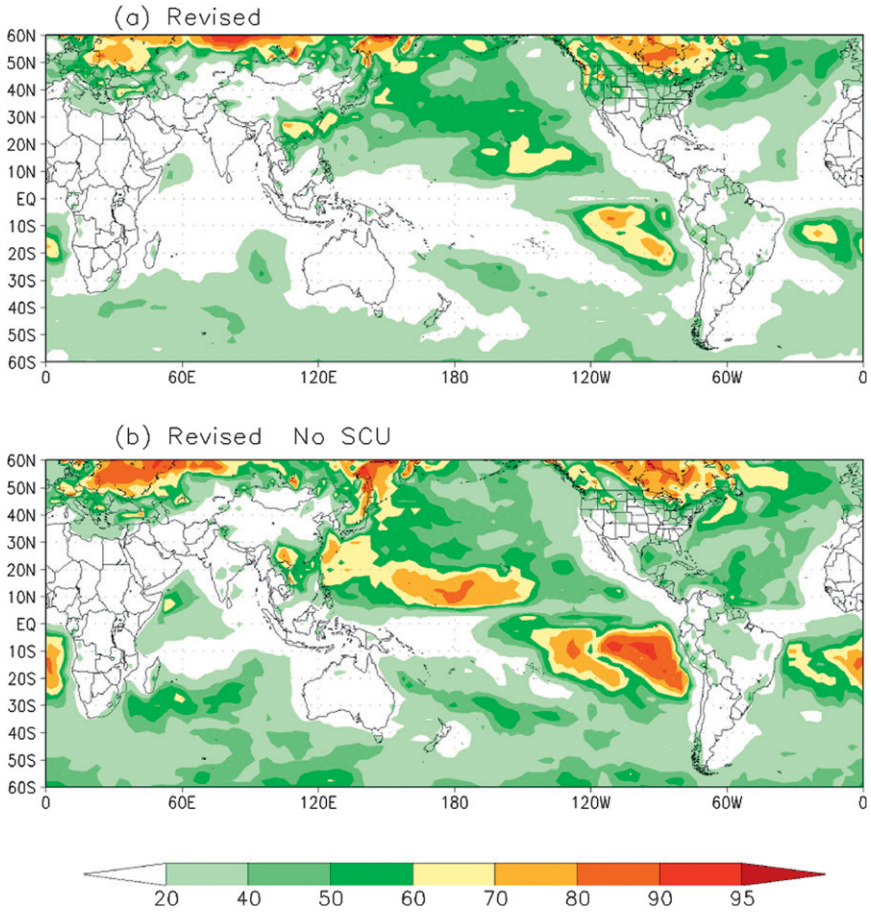

FIG. 2. As in Fig. 1, but from (a) the revised model simulation and (b) a revised model simulation without stratocumulus-cloud-top-driven turbulence mixing.

monthly mean depth of cumulus clouds. Considering the threshold cloud depth to be 150 hPa to distinguish deep and shallow convection, Fig. 5 indicates that most of the shallow cumulus convection occurs in the trade wind areas of the Pacific Ocean and in regions farther out to sea than the stratocumulus regions off the west coasts of America and Africa.

b. Medium-range forecasts with data assimilation

To assess the impacts of the new schemes on forecast skill, 7-day forecasts for the period of 2 June–10 November 2008 using the NCEP Global Data Assimilation System (GDAS) were conducted. The GFS used in this test has 64 vertical sigma-pressure hybrid layers and T382 horizontal resolution, the same as the previous operational version. A spinup series of forecasts for the previous 19 days has been discarded from the analysis. Results from the GFS using the old PBL, shallow and deep convection schemes are presented as the control.

Before assessing the forecast performance of the revised model, an example of how the revised model reduces gridpoint storms (a long-standing GFS problem during the convective season as mentioned in the introduction) is presented in Figs. 6 and 7. The gridpoint storm problems have been reported with fully explicit approaches in mesoscale models (where only grid-scale condensation and precipitation are allowed and no subgrid-scale clouds are accounted for) especially in the presence of high convective instability (Molinari and Dudek 1992; Zhang et al. 1988). Using a 25-km grid spacing, for example, Zhang et al. (1988) noted that a fully explicit approach produced too much rain and a too intense surface mesolow in a mesoscale convective complex case. They argued that cumulus parameterization was required for even 10-km grid spacing. However, Fig. 6 indicates that if a cumulus parameterization scheme is not efficient enough to eliminate the convective instability, a gridpoint storm can still develop (e.g., see the unrealistic heavy precipitation in southern Alabama in Fig. 6b). The revised model (Fig. 6c) helps reduce the excessive precipitation in southern Alabama and predicts precipitation amounts similar to those observed (Fig. 6a).

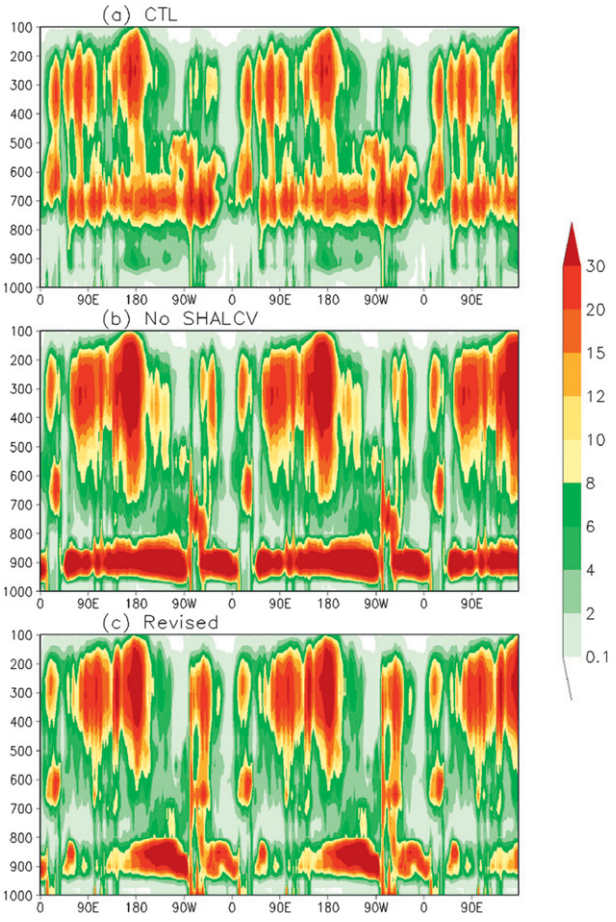

FIG. 3. Vertical cross section of mean cloud water (mg kg^{-1}) averaged over 10°S–10°N for January 2003 from the (a) control simulation, (b) control simulation without triggering shallow convection, and (c) revised model simulation.

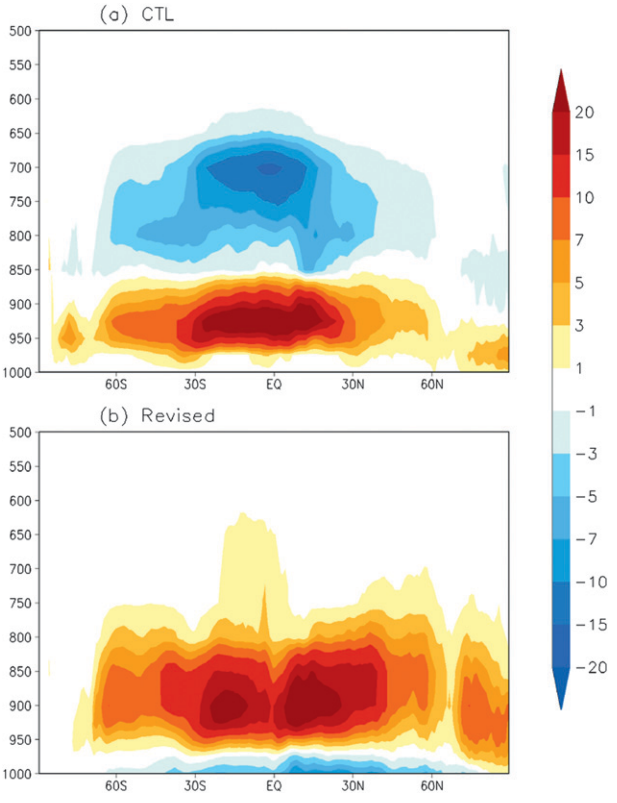

FIG. 4. Zonally averaged heating rates (10^{-6} K s^{-1}) due to the shallow convection for January 2003 from the (a) control and (b) revised model simulations.

Figures 7a and 7c show that the unrealistic gridpoint storm in southern Alabama is mainly from grid-scale precipitation, indicating that the old convective parameterization is not fully eliminating the instability that causes an explicit convective ascent on the grid scale. Figures 7b and 7d show that the realistically forecasted precipitation in southern Alabama with the revised model is mainly from convective precipitation, indicating that the revised deep convection scheme with its larger cloud-base mass flux and higher cloud tops has effectively eliminated the instability, suppressing the gridpoint storm.

A comparison of anomaly correlations and root-mean-square errors (RMSEs) for the 500-hPa height as a function of forecast length for both the Northern (20°–80°N) and Southern (20°–80°S) Hemispheres is shown in Fig. 8. In the Northern Hemisphere, the mean anomaly correlations are higher throughout the 7 days of the revised model forecast. In the Southern Hemisphere, the correlations are better for the revised model up to day 5, but are worse in the day 7 forecast. The RMSE is consistent with the anomaly correlation (i.e., if the anomaly correlation score is higher, the RMSE is lower). The better results in the Northern Hemisphere appear to reflect an improvement in the revised model convection schemes since the experiments were mostly conducted for the Northern Hemisphere summer and fall.

The RMSE for the tropical (20°S–20°N) 850- and 200-hPa vector winds is shown in Fig. 9. For the 850-hPa vector wind (Fig. 9a), RMSE is substantially reduced throughout the 7 days of the revised model forecast. At 200 hPa (Fig. 9b), the revised model score is also generally improved except for the day 1 and 2 forecasts. Although not shown in the figures, the vector wind RMSEs for both the Northern and Southern Hemispheres were also reduced with the revised model over the entire atmospheric layer throughout all forecast hours.

Comparisons of equitable threat and bias scores for the 12–36-h precipitation forecasts over the continental United States are shown in Fig. 10. The equitable threat score (Fig. 10a; Gandin and Murphy 1992) is better with

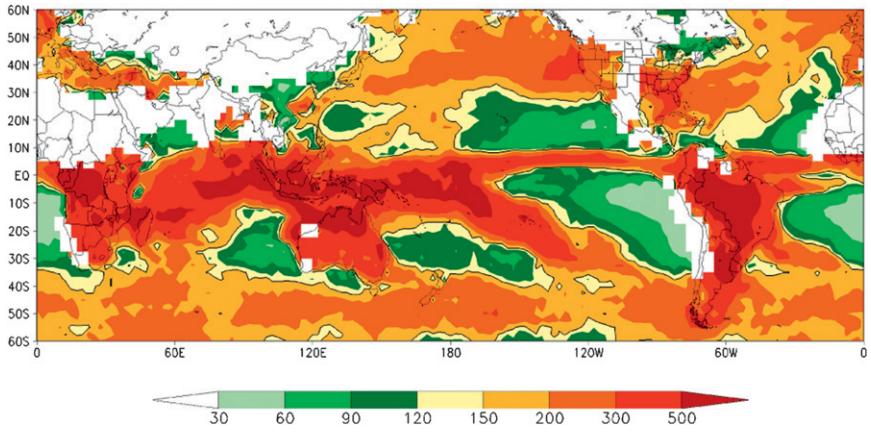

FIG. 5. Monthly mean convective cloud depth (hPa) from the revised model simulation. The thick solid contour indicates the 150-hPa cloud depth.

the revised model at higher thresholds while it is slightly worse for very light rain (a threshold of 0.2 mm day^{-1}). The lower revised model score for very light rain appears to be associated with the wetter bias as seen in Fig. 10b. Figure 10b shows that while the revised model is drier than the control except for very light rain, it has a much better bias score (bias score is better if it is closer to 1.0) at the very high thresholds. This indicates that the revised model has largely suppressed the unrealistic gridpoint storms seen in Fig. 6. The forecast skill for the 12–36- and 36–60-h precipitation forecasts were similar to those in the 12–36-h precipitation forecasts (not shown).

The performance of the revised model against the old GFS for hurricane forecasts is shown in Fig. 11 in terms of hurricane track and intensity errors, respectively. As shown in Figs. 11a and 11b, hurricane track forecasts with the revised model had a quite large improvement for both 2008 Atlantic and eastern Pacific hurricanes through the entire 5-day forecast. This improvement is consistent with the improvement in wind forecasts described above. Hurricane intensity forecasts (Figs. 11c and 11d) were also improved with the revised model, except for a slight degradation in Atlantic hurricanes for earlier forecast times (before 24 h). The improvement in the hurricane intensity forecasts appears to be mainly

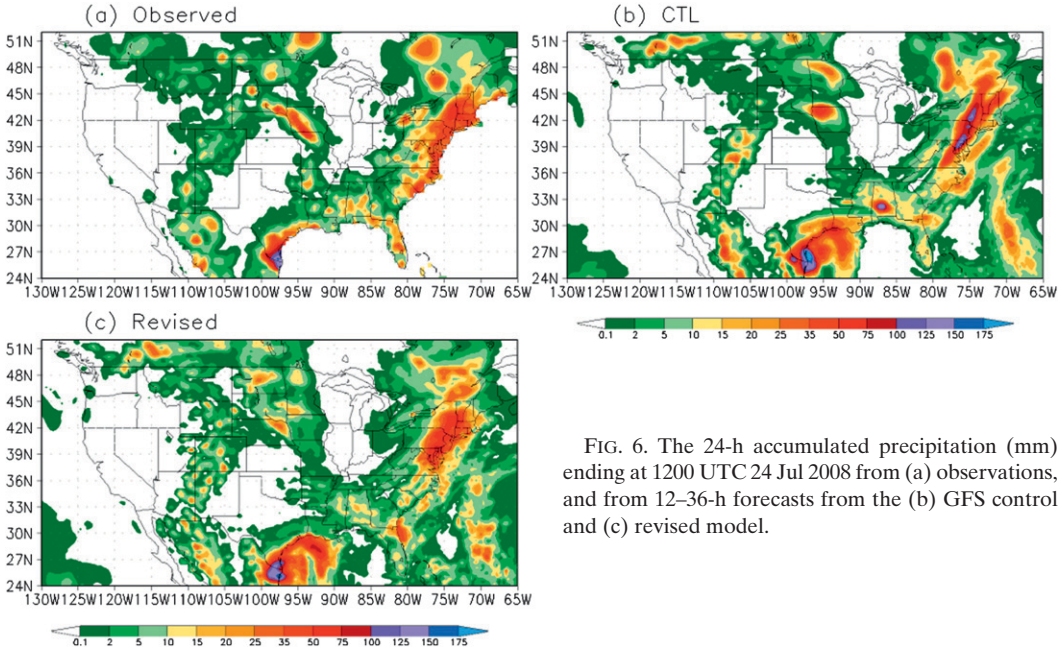

FIG. 6. The 24-h accumulated precipitation (mm) ending at 1200 UTC 24 Jul 2008 from (a) observations, and from 12–36-h forecasts from the (b) GFS control and (c) revised model.

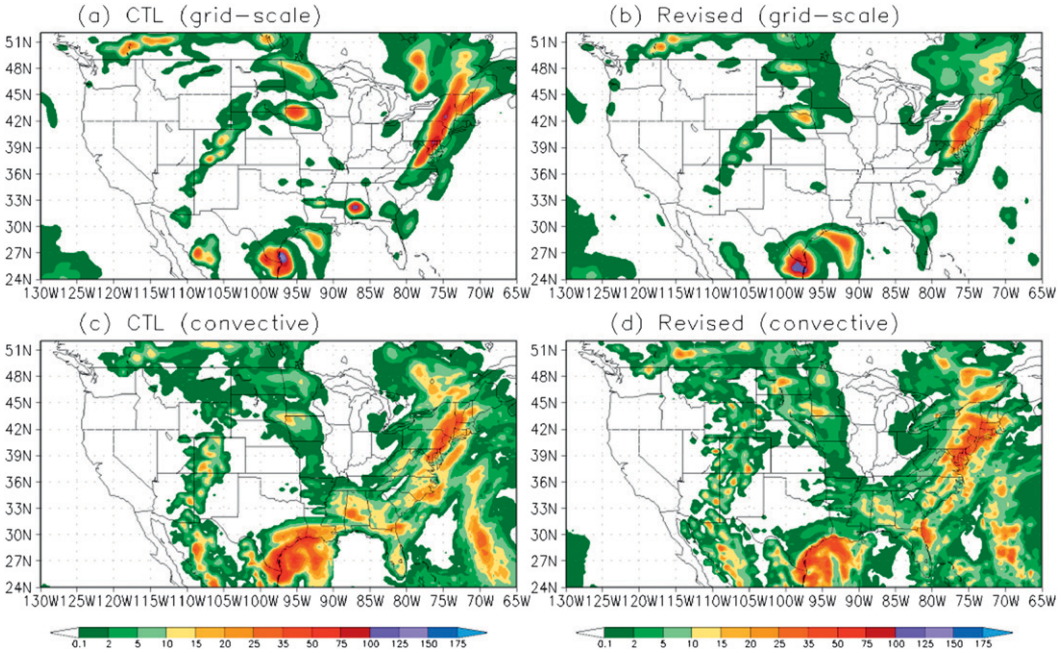

FIG. 7. As in Figs. 6b and 6c, but for (a),(b) the grid-scale and (c),(d) convective precipitation.

due to reduced convective momentum mixing in the revised convection schemes as described in section 2a(3). This is consistent with Han and Pan's (2006) study, which showed that the increased hurricane intensities due to reduced convective momentum mixing in the GFS improve the hurricane intensity forecast skill because the hurricane intensities in the GFS forecasts are generally weaker compared to the observations.

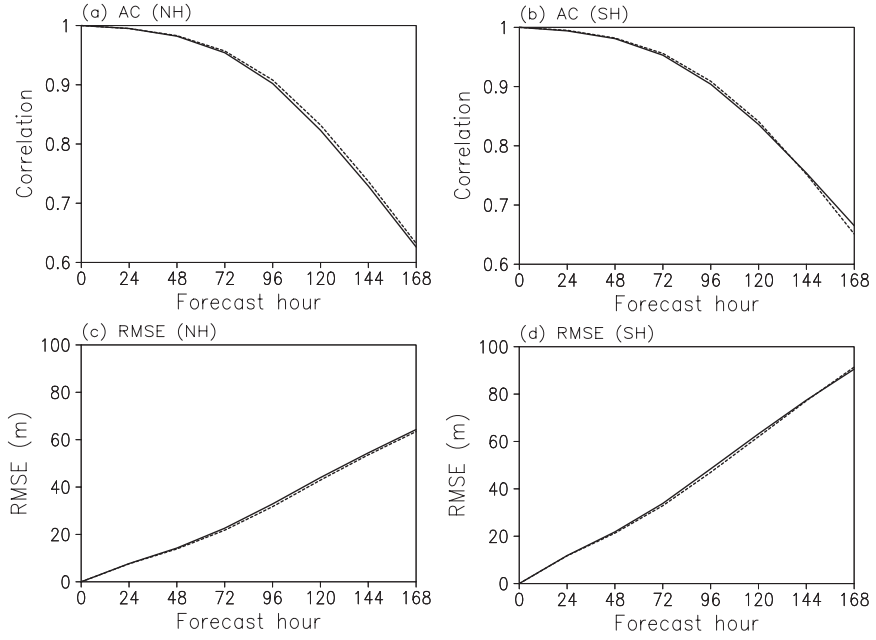

FIG. 8. (a),(b) Mean anomaly correlations and (c),(d) RMSEs of 500-hPa height for (left) the Northern Hemisphere (20°–80°N) and (right) Southern Hemisphere (20°–80°S) from the control (solid line) and revised (dashed line) model forecasts during 20 Jun–10 Nov 2008.

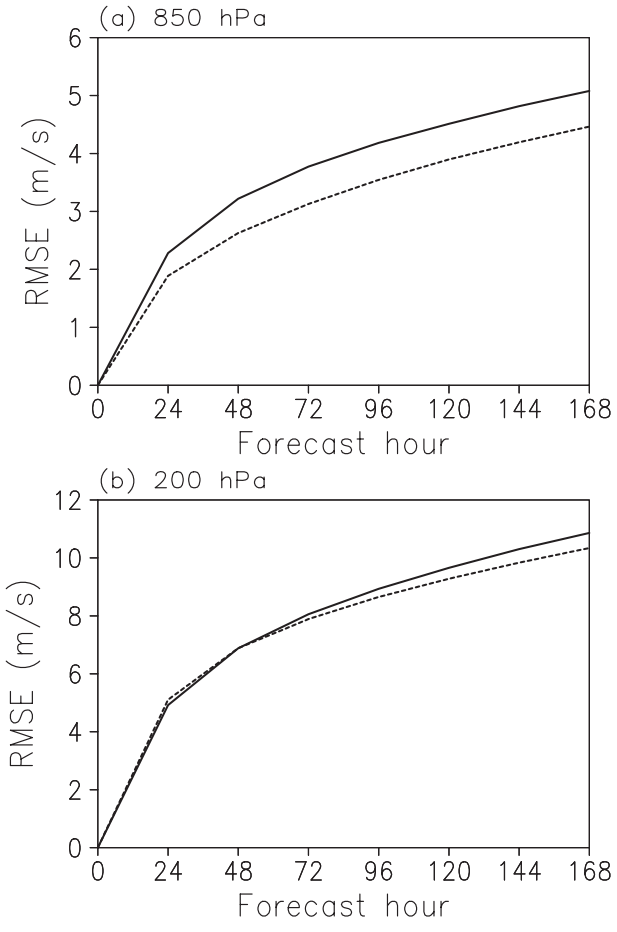

FIG. 9. As in Fig. 8, but for RMS vector wind errors (m s^{-1}) at (a) 850 and (b) 200 hPa over the tropics (20°S–20°N).

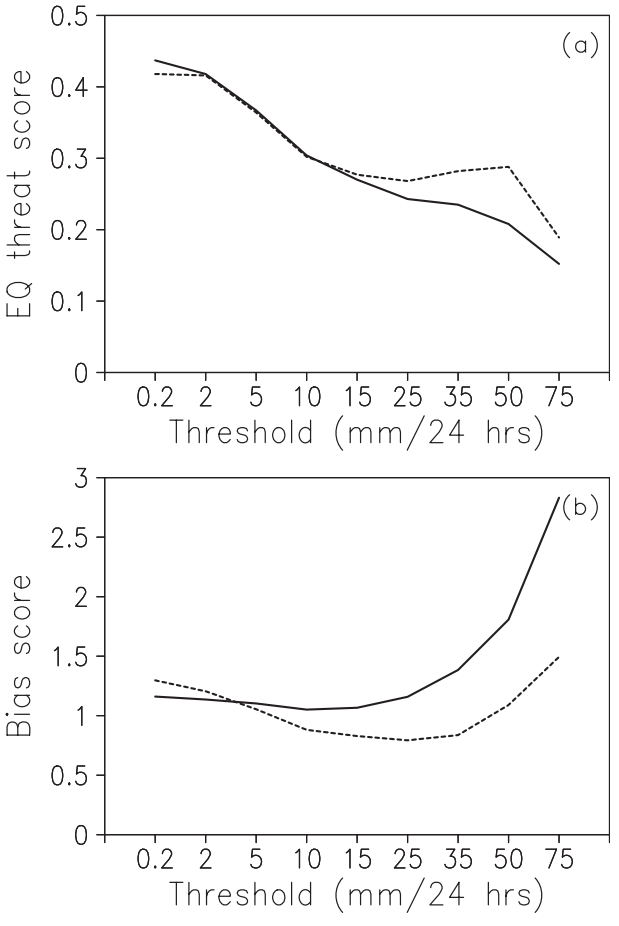

FIG. 10. As in Fig. 8, but for (a) equitable threat score and (b) bias score for the 12–36-h precipitation forecasts over the continental United States.

4. Summary and conclusions

The new physics package containing revised convection and PBL schemes and its impacts on the NCEP GFS have been described. This revision was initially made in pursuit of fixing two long-standing problems in the NCEP GFS, which are the systematic underestimation of stratocumulus clouds in the eastern Pacific and Atlantic Oceans and the frequent occurrence of unrealistic excessive heavy precipitation, the so-called gridpoint storms. The new SC scheme employs a mass flux parameterization, which is more physically appropriate than the old (turbulent diffusion) scheme. Unlike in the deep convection scheme, the cloud-base mass flux in the new SC scheme is given as a function of the convective boundary layer velocity scale. For deep convection, the scheme has been revised to make cumulus convection stronger and deeper to deplete more instability from the atmospheric column and result in the suppression of excessive grid-scale precipitation. The random cloud-top selection in the SAS scheme is replaced by an entrainment rate approach with the rate being dependent on environmental moisture. The effects of the convection-induced pressure gradient force on cumulus momentum transport and convective overshooting are parameterized in both the deep and shallow convection schemes. A modification of the triggering function has also been developed. In addition, the PBL model is revised to enhance turbulence diffusion in stratocumulus regions.

A remarkable difference between the new and old SC schemes is seen in the heating or cooling behavior in the lower-atmospheric layers above the PBL. While the old SC scheme using the diffusion approach produces a pair of lower-atmospheric layers with cooling above and heating below, the new SC scheme using a mass-flux approach produces heating throughout the convection layers due to the dominance of environmental subsidence warming. In particular, the new SC scheme does not destroy stratocumulus clouds off the west coasts of

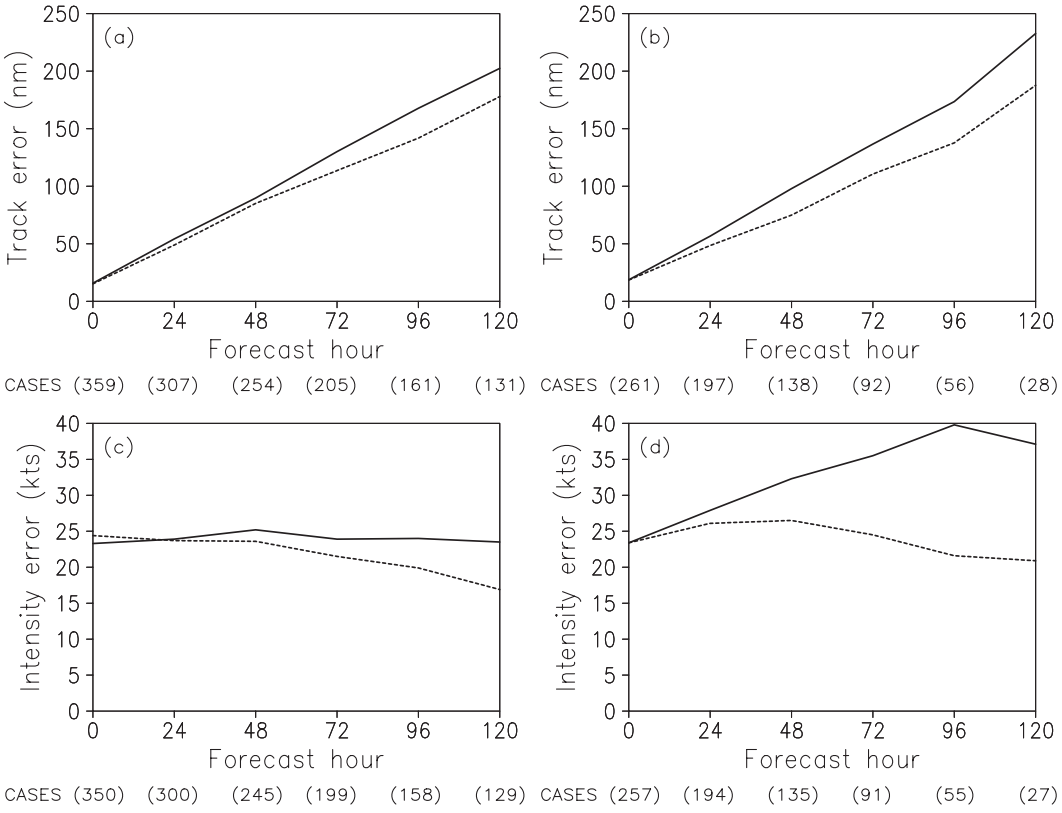

FIG. 11. As in Fig. 8, but for (a),(b) mean hurricane track errors and (c),(d) mean hurricane intensity errors for (left) Atlantic and (right) eastern Pacific Ocean regions.

South America and Africa, as the old scheme does. On the other hand, the revised deep convection scheme with its larger cloud-base mass flux and higher cloud tops appears to effectively eliminate the remaining instability in the atmospheric column that is responsible for the excessive grid-scale precipitation in the old scheme. The revised PBL scheme with its enhanced turbulence mixing in stratocumulus regions helps prevent too much low cloud from forming.

Overall, improvement, in the forecasts of global 500-hPa height, vector wind, and continental U.S. precipitation are found with the revised model. Consistent with the improvement in vector wind forecast errors, hurricane track forecasts are also improved with the revised model for both Atlantic and eastern Pacific hurricanes in 2008. In particular, hurricane intensity forecast biases are often largely reduced with increased hurricane intensity forecasts due to the reduced convective momentum mixing in the revised model.

The revised model presented in this paper was implemented operationally in the NCEP GFS in late July 2010. Since the implementation, an increase in the negative wind speed bias (lower wind speed forecasts compared to observed) throughout most of the atmosphere has been reported, resulting in weaker upper-level jet stream maxima at higher latitudes and weaker easterly wind speeds in the tropical stratosphere. This appears to be caused by the substantially increased background diffusivity for momentum. The low-level warm temperature bias over land has also increased with the reduction of atmospheric column-integrated liquid water. Tests are under way on changes to reduce those errors without degrading the forecast skill from the revised model.

For future model revisions, convective cloudiness and advanced moist turbulence parameterization are under development. The contribution to cloudiness by cumulus convection in the current revised model is indirectly taken into account by the detrainment of liquid water from convective updrafts into the grid-scale cloud water. A direct convective cloudiness contribution can be included by considering the suspended liquid water in the convective updraft. The current revised diffusion scheme has an enhanced turbulence mixing in the stratocumulus region. But it is still based on variables conserved in dry-adiabatic processes and, thus, may not be appropriate for treating cloudy layer mixing, which needs a consideration of the latent heating associated with changes of water state. In further revisions the model's turbulence

mixing will be expressed in terms of variables conserved during changes in the water state, allowing a more realistic calculation of atmospheric stability and moist turbulence mixing in cloudy regions.

Acknowledgments. The authors highly appreciate the help and many suggestions from S. Moorthi (for the GFS run), Suranjana Saha (for the CFS run), Russ Treadon (for using the GSI data assimilation system), and Fanglin Yang (for running the GFS forecasts with data assimilation and computing GFS forecast skill scores) at NCEP/EMC. Internal reviews from Peter Caplan, Fanglin Yang, Masayuki Nakagawa, and Mary Hart at NCEP/EMC are acknowledged. We are also grateful to John Ward and Steve Lord at NCEP/EMC for their encouragement on this work.

REFERENCES

Arakawa, A., and W. H. Schubert, 1974: Interaction of a cumulus cloud ensemble with the large-scale environment. Part I. *J. Atmos. Sci.,* **31,** 674–701.

Bechtold, P., M. Kohler, T. Jung, F. Doblas-Reyes, M. Leutbecher, M. J. Rodwell, F. Vitart, and G. Balsamo, 2008: Advances in simulating atmospheric variability with the ECMWF model: From synoptic to decadal time-scales. *Quart. J. Roy. Meteor. Soc.,* **134,** 1337–1351.

Caplan, P., J. Derber, W. Gemmill, S.-Y. Hong, H.-L. Pan, and D. Parrish, 1997: Changes to the 1995 NCEP operational medium-range forecast model analysis–forecast system. *Wea. Forecasting,* **12,** 581–594.

Deardorff, J. W., 1980: Cloud-top entrainment instability. *J. Atmos. Sci.,* **37,** 131–147.

de Roode, S. R., P. G. Duynkerke, and A. P. Siebesma, 2000: Analogies between mass-flux and Reynolds-averaged equations. *J. Atmos. Sci.,* **57,** 1585–1598.

Gandin, L. S., and A. H. Murphy, 1992: Equitable skill scores for categorical forecasts. *Mon. Wea. Rev.,* **120,** 361–370.

Grant, A. L. M., 2001: Cloud-base fluxes in the cumulus-capped boundary layer. *Quart. J. Roy. Meteor. Soc.,* **127,** 407–422.

——, and A. R. Brown, 1999: A similarity hypothesis for shallow cumulus transports. *Quart. J. Roy. Meteor. Soc.,* **125,** 1913–1936.

Han, J., and H.-L. Pan, 2006: Sensitivity of hurricane intensity forecast to convective momentum transport parameterization. *Mon. Wea. Rev.,* **134,** 664–674.

Hong, S.-Y., and H.-L. Pan, 1996: Nonlocal boundary layer vertical diffusion in a medium-range forecast model. *Mon. Wea. Rev.,* **124,** 2322–2339.

Jakob, C., and A. P. Siebesma, 2003: A new subcloud model for mass-flux convection schemes: Influence on triggering, updraft properties, and model climate. *Mon. Wea. Rev.,* **131,** 2765–2778.

Lock, A. P., A. R. Brown, M. R. Bush, G. M. Martin, and R. N. B. Smith, 2000: A new boundary layer mixing scheme. Part I: Scheme description and single-column model tests. *Mon. Wea. Rev.,* **128,** 3187–3199.

Louis, J. F., M. Tiedtke, and J. F. Geleyn, 1982: A short history of the PBL parameterization at ECMWF. *Proc. Workshop on Boundary-Layer Parameterization,* Reading, United Kingdom, ECMWF, 59–79.

MacVean, M. K., and P. J. Mason, 1990: Cloud-top entrainment instability through small-scale mixing and its parameterization in numerical models. *J. Atmos. Sci.,* **47,** 1012–1030.

Moeng, C.-H., P. P. Sullivan, and B. Stevens, 1999: Including radiative effects in an entrainment-rate formula for buoyancy-driven PBLs. *J. Atmos. Sci.,* **56,** 1031–1049.

Molinari, J., and M. Dudek, 1992: Parameterization of convective precipitation in mesoscale numerical models: A critical review. *Mon. Wea. Rev.,* **120,** 326–344.

Moorthi, S., H.-L. Pan, and P. Caplan, 2001: Changes to the 2001 NCEP operational MRF/AVN global analysis/forecast system. NWS Tech. Procedures Bull. 484, 14 pp.

Pacanowski, R. C., and S. M. Griffies, cited 1998: MOM 3.0 manual. NOAA/GFDL. [Available online at http://www.gfdl.noaa.gov/ocean-model.]

Pan, H.-L., and W.-S. Wu, 1995: Implementing a mass flux convective parameterization package for the NMC Medium-Range Forecast model. NMC Office Note 409, 40 pp.

Raga, G. B., J. B. Jensen, and M. B. Baker, 1990: Characteristics of cumulus band clouds off the coast of Hawaii. *J. Atmos. Sci.,* **47,** 338–355.

Randall, D. A., 1980: Conditional instability of the first kind upside-down. *J. Atmos. Sci.,* **37,** 125–130.

Rossow, W. B., and R. A. Schiffer, 1991: ISCCP cloud data products. *Bull. Amer. Meteor. Soc.,* **72,** 2–20.

Saha, S., and Coauthors, 2006: The NCEP Climate Forecast System. *J. Climate,* **19,** 3483–3517.

Siebesma, A. P., and J. W. M. Cuijpers, 1995: Evaluation of parametric assumptions for shallow cumulus convection. *J. Atmos. Sci.,* **52,** 650–666.

——, and Coauthors, 2003: A large eddy simulation intercomparison study of shallow cumulus convection. *J. Atmos. Sci.,* **60,** 1201–1219.

Stull, R. B., 1988: *An Introduction to Boundary Layer Meteorology*. Kluwer Academic, 666 pp.

Tiedtke, M., W. A. Heckley, and J. Slingo, 1988: Tropical forecasting at ECMWF: The influence of physical parameterization on the mean structure of forecasts and analyses. *Quart. J. Roy. Meteor. Soc.,* **114,** 639–644.

Troen, I., and L. Mahrt, 1986: A simple model of the atmospheric boundary layer sensitivity to surface evaporation. *Bound.-Layer Meteor.,* **37,** 129–148.

Wang, W., S. Saha, H.-L. Pan, S. Nadiga, and G. White, 2005: Simulation of ENSO in the new NCEP Coupled Forecast System model (CFS03). *Mon. Wea. Rev.,* **133,** 1574–1593.

Xu, K.-M., and D. A. Randall, 1996: A semiempirical cloudiness parameterization for use in climate models. *J. Atmos. Sci.,* **53,** 3084–3102.

Zhang, D.-L., E.-Y. Hsie, and M. W. Moncrieff, 1988: A comparison of explicit and implicit predictions of convective and stratiform precipitating weather systems with a meso-β-scale numerical model. *Quart. J. Roy. Meteor. Soc.,* **114,** 31–60.

Zhang, G. J., and X. Wu, 2003: Convective momentum transport and perturbation pressure field from a cloud-resolving model simulation. *J. Atmos. Sci.,* **60,** 1120–1139.